Supplement figures

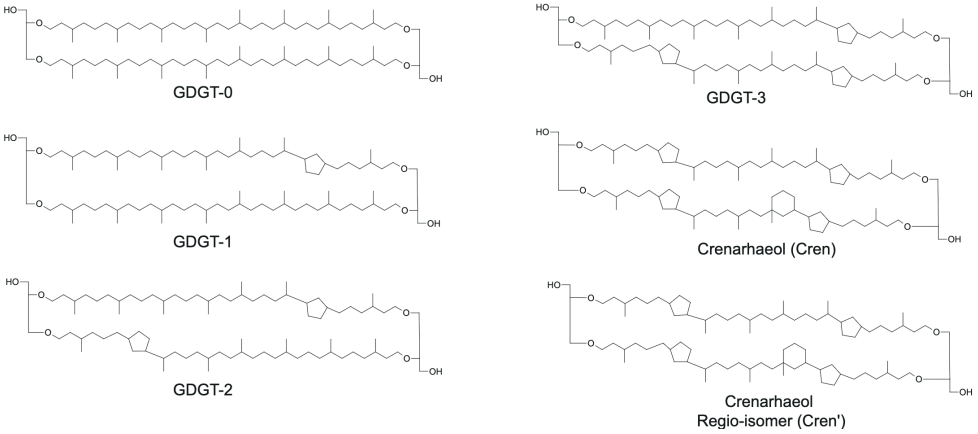

Figure. S1: Molecular structure of isoprenoid GDGTs.

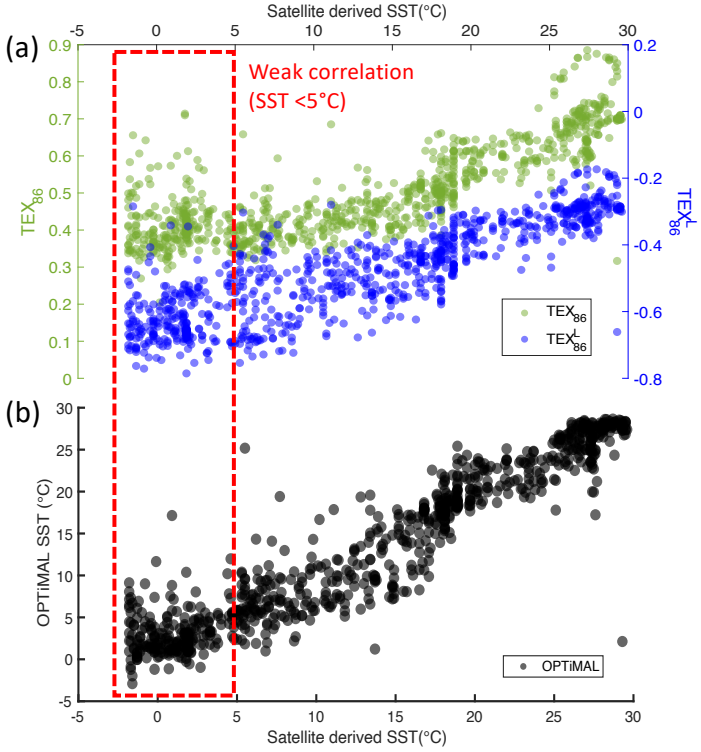

Figure. S2: Correlation of (a)TEX_{86} index, TEX_{86}^{L} index, and (b) OPTiMAL SST in the global core-top samples with satellite-derived SSTs (n = 907). Green circles: TEX_{86} index, blue circles: TEX_{86}^{L} index, black circles: OPTiMAL SST.

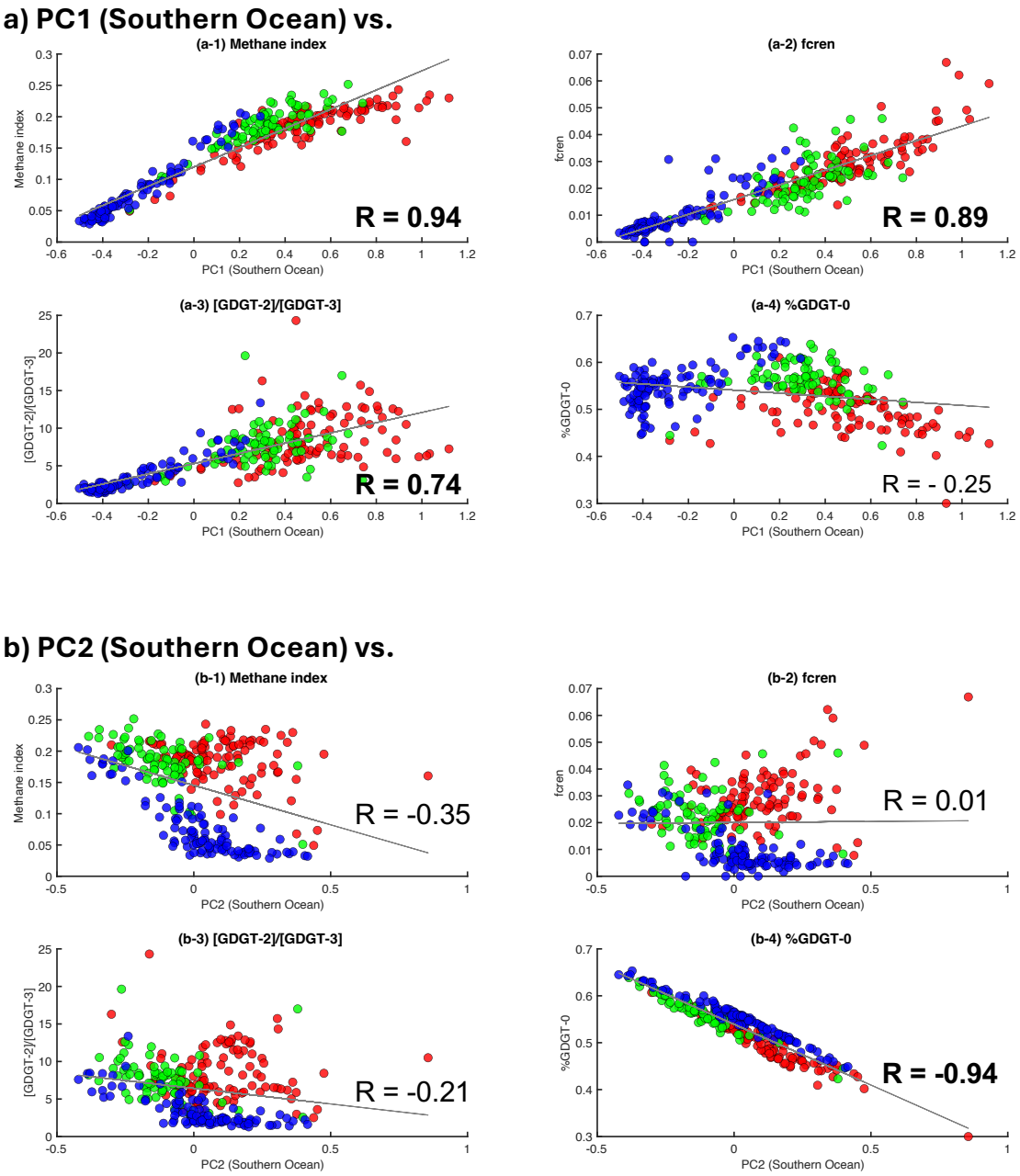

Figure S3: Scatter plots of PC1 (a) and PC2 (b) versus (1) Methane Index, (2) fcren, (3) [GDGT-2]/[GDGT-3], and (4) %GDGT-0 in Southern Ocean core-top GDGT data (n = 289). Core-top values are classified into three groups based on frontal positions: southern ACC (blue circles), central ACC (green circles), and northern ACC (red circles), as defined by the SBF and SAF (Fig. 4c).

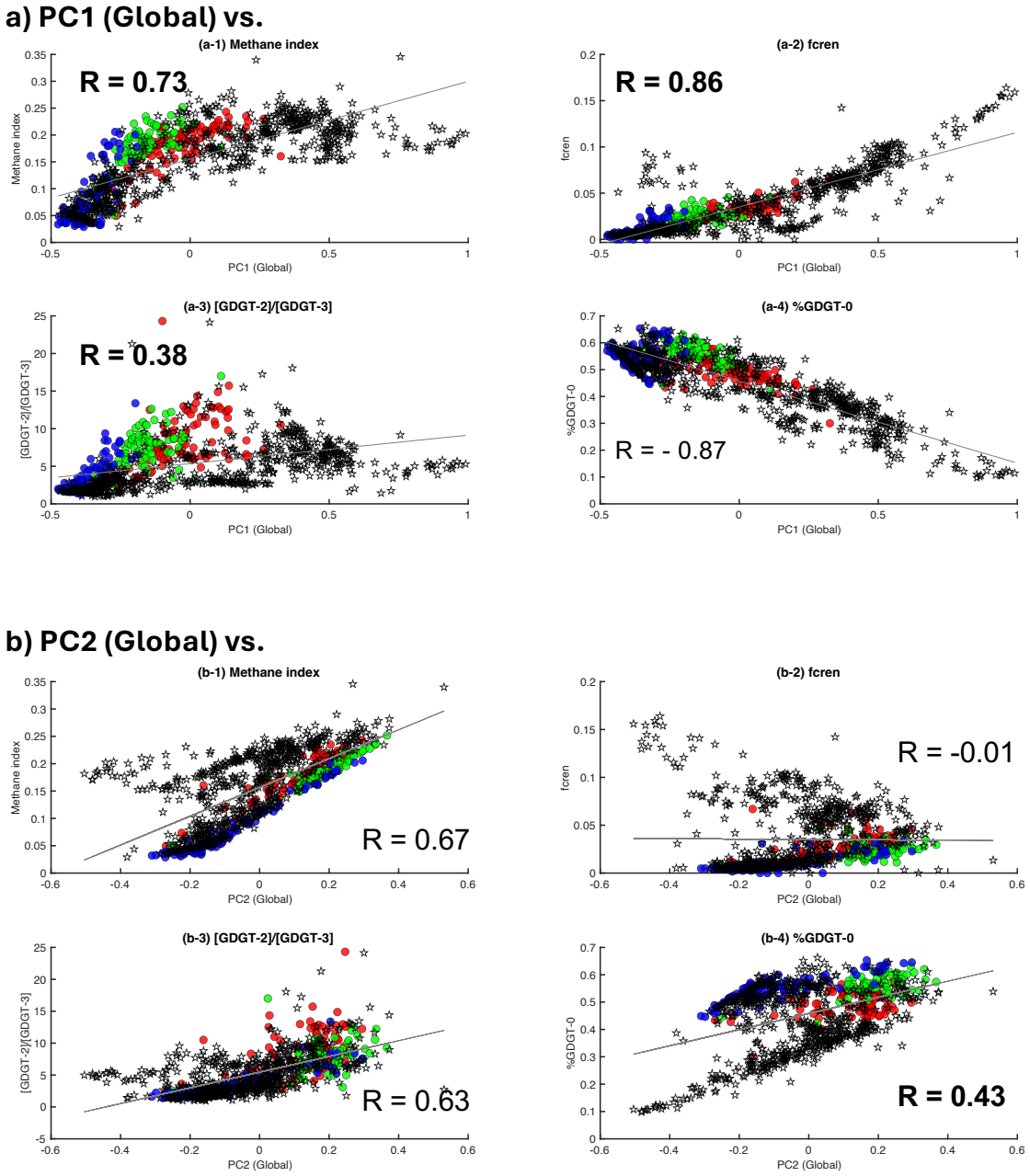

15 **Figure. S4: Scatter plot of the global a) PC1 and b) PC2 versus (1) Methane Index, (2) fcren, (3) [GDGT-2]/[GDGT-3], (4) %GDGT-0 in the Global core top GDGT data (*n* = 916). The core-top values are classified into three groups: south of the ACC (blue circle), centre of the ACC (green circle) and north of the ACC (red circle), as defined by the SBF and SAF The global core-top are shown as stars.**

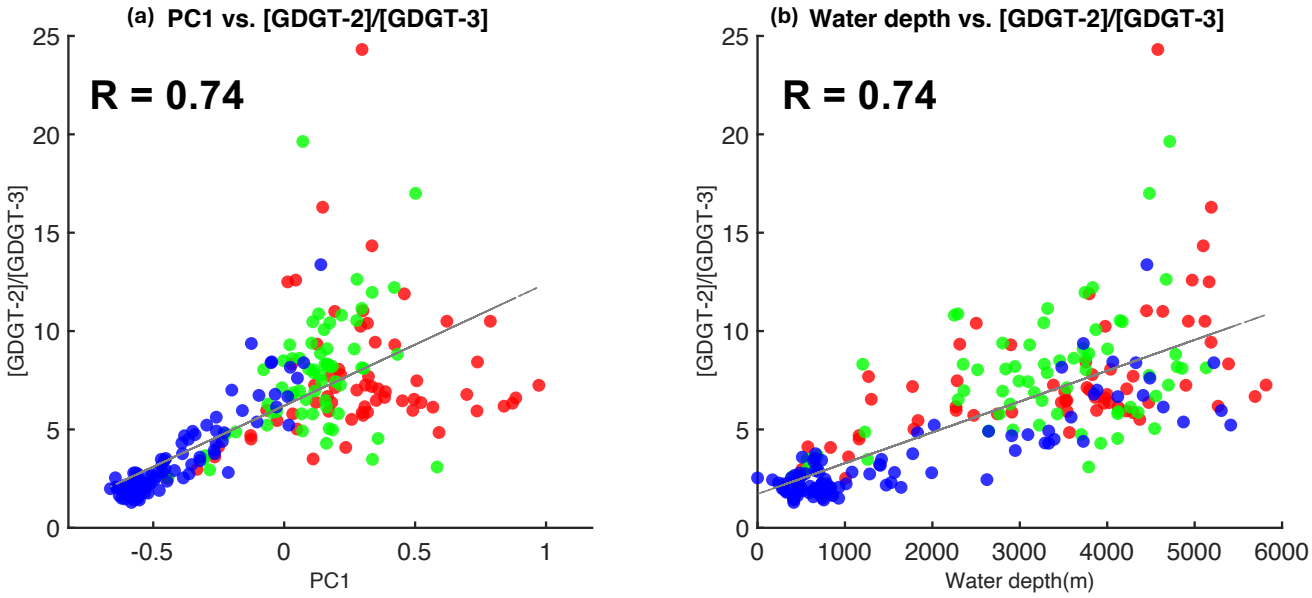

Figure. S5: Scatter plot of [GDGT-2]/[GDGT-3] versus (a) PC1 (*n* = 289) and (b) water depth (*n* = 236) in the Southern Ocean dataset. The core-top values are classified into three groups: south of the ACC (blue circles), centre of the ACC (green circles) and north of the ACC (red circles), as defined by the SBF and SAF (shown in Fig: 4c).

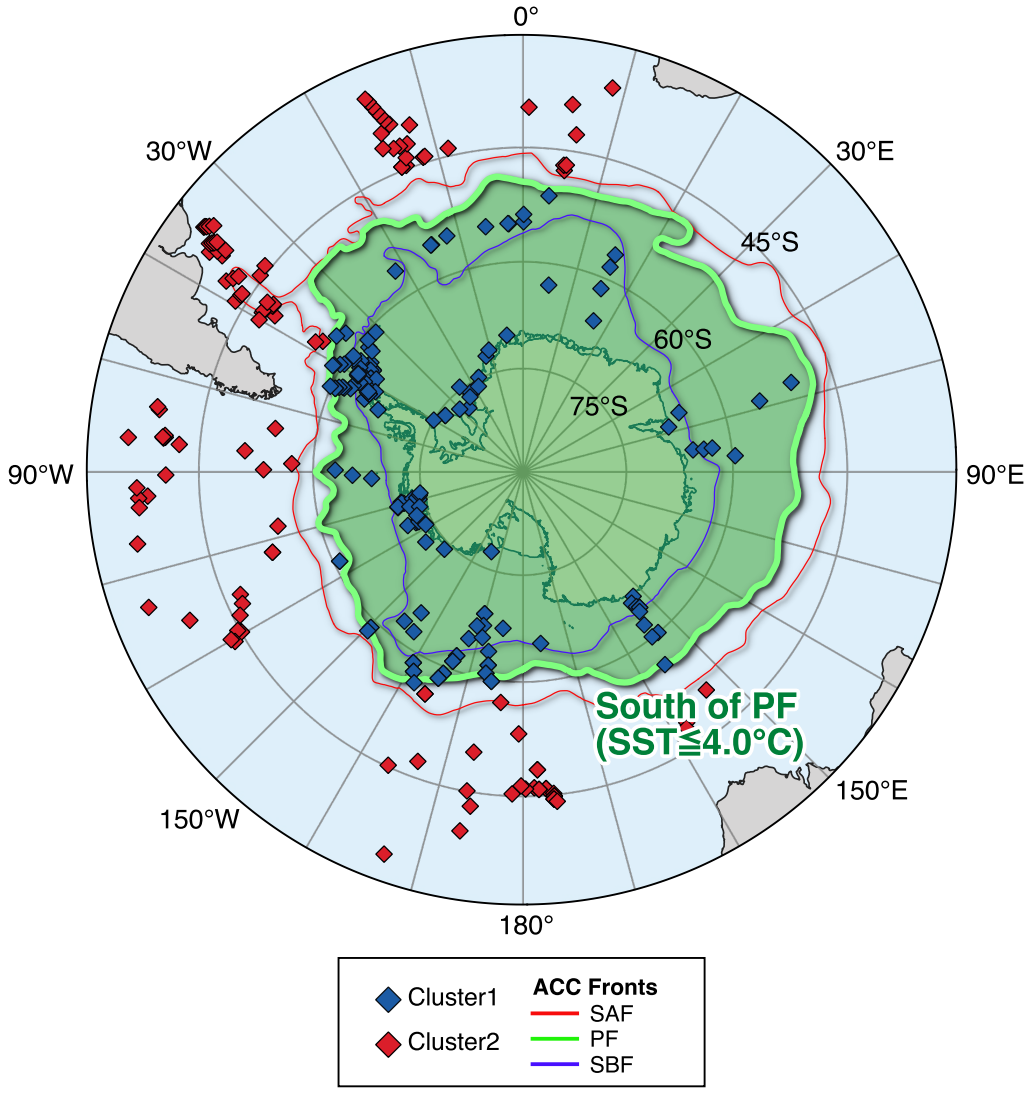

25 **Figure. S6: Map showing the area south of the PF where the AIZ index can be used as palaeothermometry. Red diamonds represent the sites north of the PF, while blue diamonds represent the sites south of the PF.**

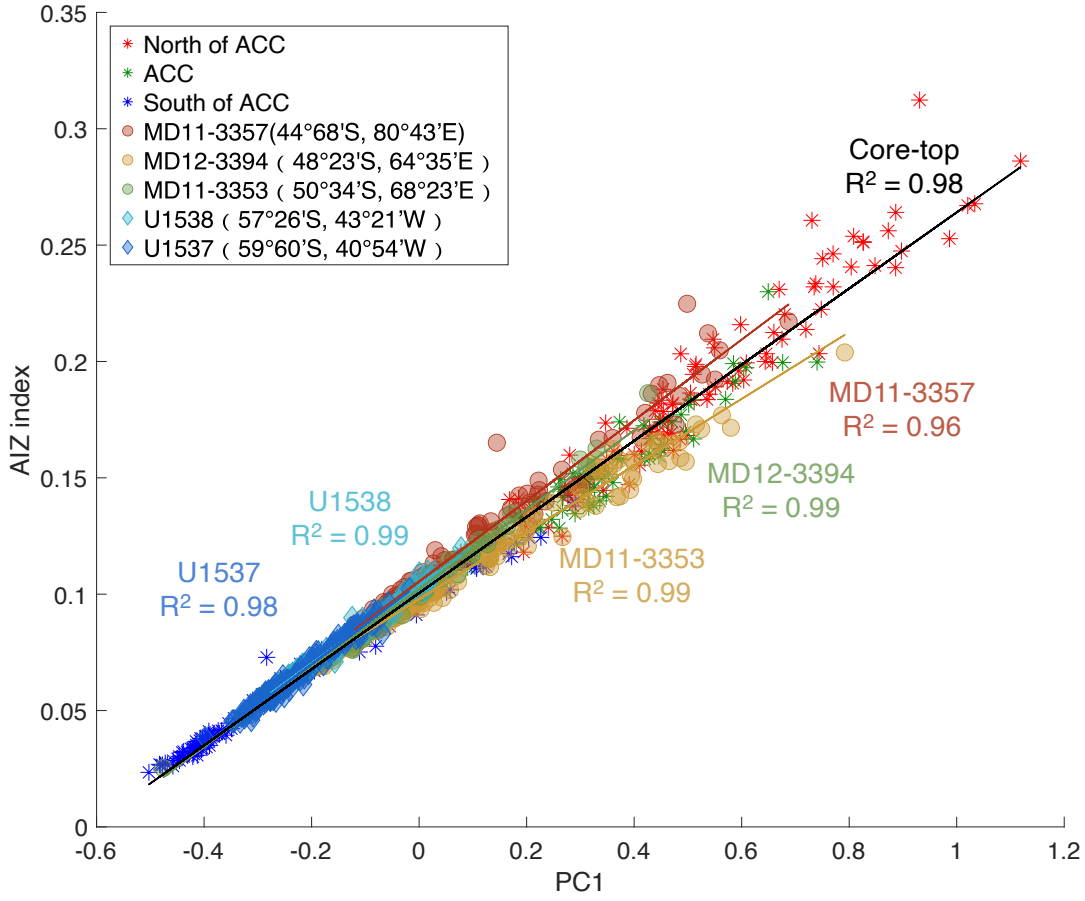

Figure. S7: Scatter plot of PC1 versus AIZ index in the Southern Ocean core-top samples and five sediment cores spanning the last 160 kyr. Core-top samples are classified by position relative to the ACC: red asterisks (north of the ACC), green asterisks (centre of the ACC), blue asterisks (south of the ACC). Sediment cores: dark red circles (MD11-3357), dark yellow circles (MD12-3394), green circles (MD11-3353), and light blue diamonds (U1538), blue diamonds (U1537).

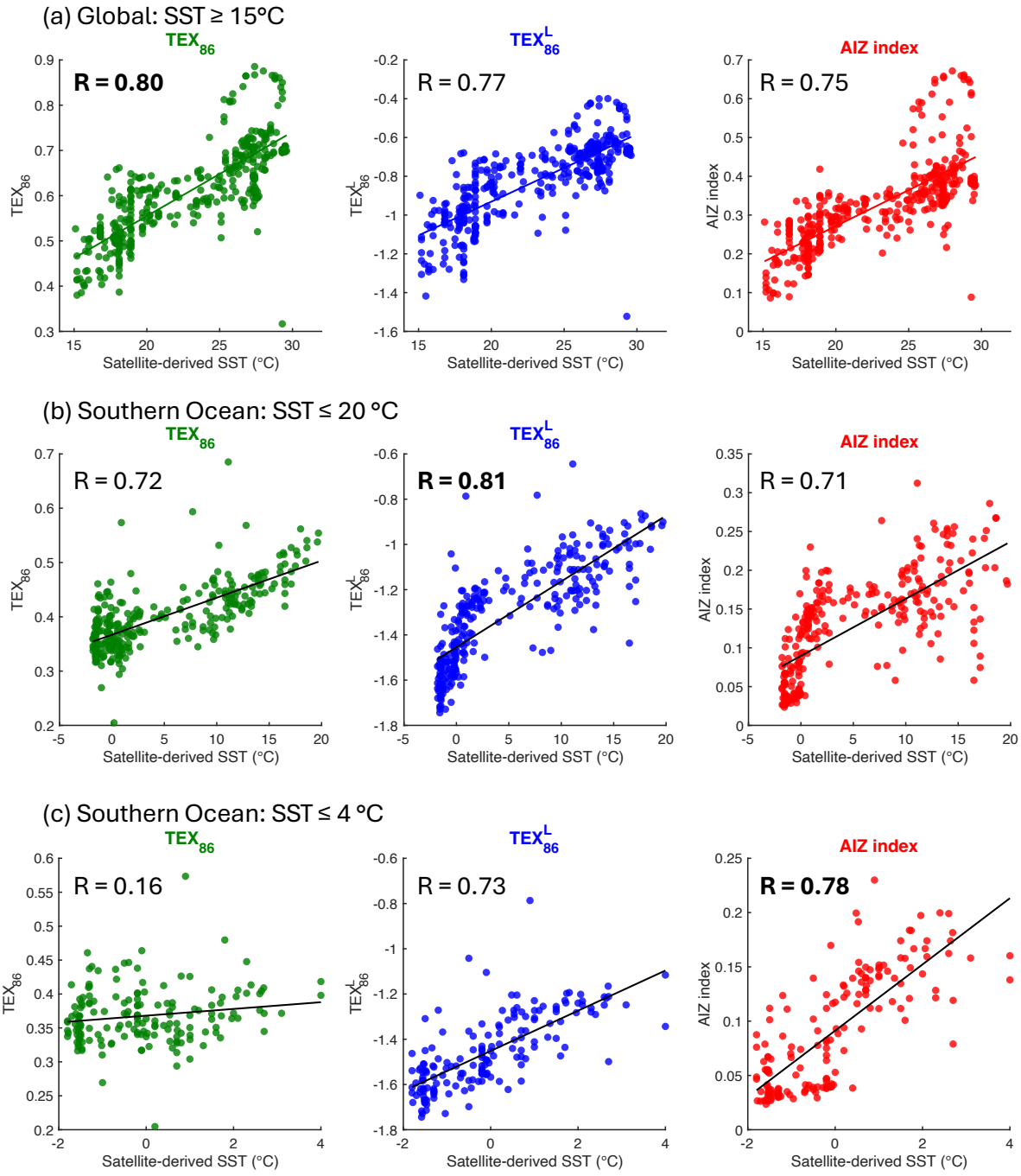

Figure. S8: Comparison of isoGDGT-based temperature proxies (TEX_{86}, TEX_{86}^{L}, and AIZ index) with satellite-derived SST across global and the Southern Ocean core-top datasets. Temperature ranges: (a) global sites ≥ 15 °C, (b) Southern Ocean sites ≤ 20 °C, and (c) Southern Ocean sites ≤ 4 °C. Symbols represent: green circles = TEX_{86}, blue circles = TEX_{86}^{L}, red circles = AIZ index (this study).

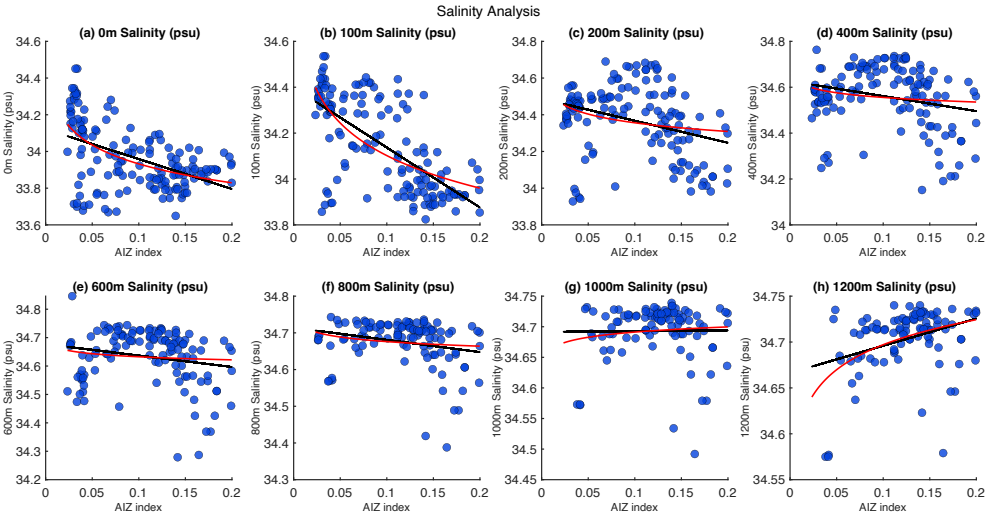

Figure. S9: Scatter plot of core-top AIZ index versus satellite-derived in situ annual salinity (psu) at various depths (0–1200 m) south of the PF (n = 96–168). Linear calibration lines are shown in black, and nonlinear calibration curves are shown in red.

Table S1: Coefficients of determination (R^2) between AIZ values and salinity at different depths in different seasons at sites south of PF.

Season / Depth	0 m (n = 149)	100 m (n = 144)	200 m (n = 143)	400m (n = 132)	600m (n = 122)	800m (n = 107)	1000m (n = 98)	1200m (n = 96)
Annual	0.22 (0.28)	**0.45 (0.42)**	0.11 (0.05)	0.06 (0.02)	0.04 (0.01)	0.05 (0.02)	0.0001 (0.01)	0.11 (0.18)
Summer (Jan–Mar)	0.33 (0.32)	**0.40 (0.37)**	0.07 (0.02)	0.07 (0.03)	0.04 (0.01)	0.07 (0.03)	0.0003 (0.01)	0.10 (0.16)
Autumn (Apr–June)	0.34 (0.42)	**0.45 (0.43)**	0.13 (0.07)	0.03 (0.00)	0.03 (0.00)	0.04 (0.01)	0.001 (0.02)	0.11 (0.18)
Winter (July–Sep)	0.01 (0.04)	**0.44 (0.41)**	0.13 (0.08)	0.04 (0.01)	0.03 (0.00)	0.04 (0.01)	0.001 (0.01)	0.12 (0.20)
Spring (Oct–Dec)	0.18 (0.22)	**0.41 (0.36)**	0.08 (0.03)	0.10 (0.05)	0.05 (0.02)	0.06 (0.03)	0.0001 (0.01)	0.11 (0.17)

R^2 values for the regression lines and logarithmic curves are shown with and without brackets, respectively. The highest R^2 values in every season are shown in bold.

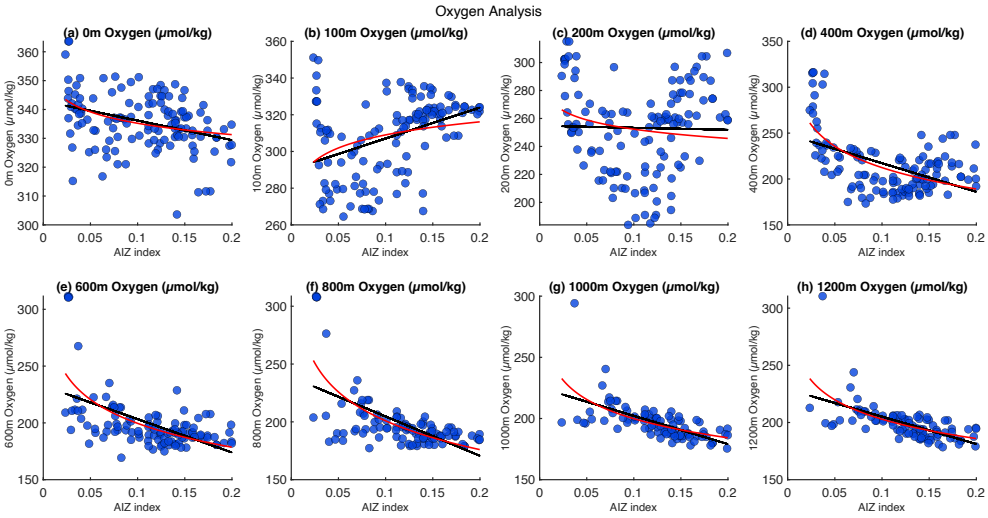

45

Figure. S10: Scatter plot of core-top AIZ index versus satellite-derived in situ annual oxygen content (µmol/kg) at various depths (0–1200 m) south of the PF (*n* = 96–168). Linear calibration lines are shown in black, and nonlinear calibration curves are shown in red.

50 **Table S2: Coefficients of determination (R^2) between AIZ values and oxygen saturation at different depths in different seasons at sites south of PF.**

Season / Depth	0 m (*n* = 149)	100 m (*n* = 144)	200 m (*n* = 143)	400m (*n* = 132)	600m (*n* = 122)	800m (*n* = 107)	1000m (*n* = 98)	1200m (*n* = 96)
Annual	0.12 (0.12)	0.16 (0.08)	0.0005 (0.03)	0.23 (0.39)	0.29 (0.41)	0.35 **(0.48)**	**0.39** (0.38)	0.37 (0.38)
Summer (Jan–Mar)	0.05 (0.04)	0.15 (0.09)	0.02 (0.06)	0.21 (0.32)	0.28 (0.38)	**0.32** **(0.47)**	0.29 (0.28)	0.30 (0.31)
Autumn (Apr–June)	0.03 (0.03)	0.30 (0.23)	0.04 (0.003)	0.15 (0.27)	0.32 **(0.44)**	0.30 (0.40)	**0.42** (0.40)	0.35 (0.35)
Winter (July–Sep)	0.38 (0.37)	0.12 (0.06)	0.05 (0.15)	0.25 (0.41)	0.28 (0.41)	0.41 **(0.55)**	**0.43** (0.42)	0.40 (0.42)
Spring (Oct–Dec)	0.32 (0.30)	0.01 (0.0002)	0.004 (0.003)	0.24 (0.40)	0.21 (0.30)	0.33 **(0.46)**	0.37 (0.34)	**0.38** (0.40)

R^2 values for the regression lines and logarithmic curves are shown with and without brackets, respectively. The highest R^2 values in every season are shown in bold.